A split-beam probe-pump-probe scheme for femtosecond time resolved protein X-ray crystallography

Jasper J. van Thor and Anders Madsen

Citation: Structural Dynamics **2**, 014102 (2015); doi: 10.1063/1.4906354
View online: http://dx.doi.org/10.1063/1.4906354
View Table of Contents: http://scitation.aip.org/content/aca/journal/sdy/2/1?ver=pdfcov
Published by the American Crystallographic Association, Inc.

A split-beam probe-pump-probe scheme for femtosecond time resolved protein X-ray crystallography

Jasper J. van Thor[1,a)] and Anders Madsen[2]
[1]*Division of Molecular Biosciences, Imperial College London, South Kensington Campus. SW7 2AZ London, United Kingdom*
[2]*European X-Ray Free-Electron Laser Facility, Albert-Einstein-Ring 19, 22761 Hamburg, Germany*

(Received 30 August 2014; accepted 9 January 2015; published online 30 January 2015)

In order to exploit the femtosecond pulse duration of X-ray Free-Electron Lasers (XFEL) operating in the hard X-ray regime for ultrafast time-resolved protein crystallography experiments, critical parameters that determine the crystallographic signal-to-noise ($I/\sigma I$) must be addressed. For single-crystal studies under low absorbed dose conditions, it has been shown that the intrinsic pulse intensity stability as well as mode structure and jitter of this structure, significantly affect the crystallographic signal-to-noise. Here, geometrical parameters are theoretically explored for a three-beam scheme: X-ray probe, optical pump, X-ray probe (or "probe-pump-probe") which will allow experimental determination of the photo-induced structure factor amplitude differences, ΔF, in a ratiometric manner, thereby internally referencing the intensity noise of the XFEL source. In addition to a non-collinear split-beam geometry which separates un-pumped and pumped diffraction patterns on an area detector, applying an additional convergence angle to both beams by focusing leads to integration over mosaic blocks in the case of well-ordered stationary protein crystals. Ray-tracing X-ray diffraction simulations are performed for an example using photoactive yellow protein crystals in order to explore the geometrical design parameters which would be needed. The specifications for an X-ray split and delay instrument that implements both an offset angle and focused beams are discussed, for implementation of a probe-pump-probe scheme at the European XFEL. We discuss possible extension of single crystal studies to serial femtosecond crystallography, particularly in view of the expected X-ray damage and ablation due to the first probe pulse. [http://dx.doi.org/10.1063/1.4906354]

I. BACKGROUND

Structural dynamics in the crucial early time scales of biological activation are directly linked to macromolecular function. Traditionally, our knowledge of photo-induced coherent wavepacket motion in biological materials has come from ultrafast spectroscopy. It would be a genuine breakthrough to directly observe such processes in proteins in real time and in real coordinate space, using X-ray crystallography. This manuscript addresses the technical question how x-ray free-electron lasers (XFEL) sources may be successfully used to directly visualise coherent femtosecond excited state nuclear dynamics by X-ray diffraction. An example of such coherent wavepacket motion in a biological photoreceptor is the photoisomerisation of the p-coumaric acid chromophore of the Photoactive Yellow Protein (PYP).[1] The associated time-constant ~500 fs is on the order, or shorter than, vibrational dephasing and its fundamental frequency is close to that of the torsional mode which has significant projection on the reactive

[a)]Author to whom correspondence should be addressed. Electronic mail: j.vanthor@imperial.ac.uk

coordinate. The experimental ability to achieve femtosecond time resolved protein X-ray crystallography yet needs to be demonstrated. In order to realize this capability, successful pump-probe X-ray crystallography studies done at synchrotron stations with picosecond time resolution[2–11] must be extended to the femtosecond time regime at XFELs. Opportunities for theory development in this area are compelling. It is now well established that protein X-ray crystallography with near atomic resolution is possible with XFELs, although currently primarily focused on microcrystals and Monte-Carlo crystallographic integration approaches,[12–16] referred to as Serial Femtosecond Crystallography (SFX). Several studies have pioneered the Coulombic explosion and radiation damage[3,12,17,18] and peak power tolerance of small, micron sized, and also large crystals. SFX can allow radiation-damage free measurements which can be critical for instance in cases where proteins include redox active transition metal centers such as photosystem II.[19]

Recently, successful time resolved applications of SFX have been reported.[15,16] A key characteristic has been the use of nanosecond photolysis, which significantly increases concentrations of reaction intermediates as compared to femtosecond optical excitation.[20] A femtosecond time resolved SFX measurement of light sensitive protein crystals will therefore require increased accuracy of the measured photo-induced structure factor amplitude differences ΔF's as compared to nanosecond photolysis. Published experimental evidence has demonstrated that a Monte-Carlo method can be successfully used to detect anomalous scattering, requiring no further monochromatisation when used in Self-Amplified Spontaneous Emission (SASE) mode, if a sufficient number of frames (millions) are collected and merged.[14,21] Through extensive averaging a Monte-Carlo integration of many observations overcomes the uncertainty in photon energy and its spread, intensity, and mode structure as well as partiality. Considering however the phasing power of the data collected having intensity differences on the order of 20%,[21] the higher signal-to-noise ratio required for a successful femtosecond pump-probe measurement suggests that many more frames would need to be processed. An alternative approach seeks to apply monochromatic X-ray crystallography using large single crystals under conditions of low absorbed dose. In order to select the energy in SASE mode a monochromator should be used, or alternatively the XFEL can be used in self-seeded mode. This paper considers such low dose conditions, which have already been characterized.[22]

In this manuscript, we explore an internally referenced crystallography method which uses two angular offset beams (non-collinear) to record both un-pumped and pumped diffraction patterns in single frames that can be integrated separately because the shifted beam centers spatially separate the Bragg spots. In Sec. II, we review the critical issue of accuracy of the ΔF determination when pump-probe measurements are made using an XFEL source. Section III discusses the basic geometry of an internally referenced split-beam non-collinear method. We show that additionally applying the Convergent Beam Method (CBM), ratiometric detection of photoinduced structure factor differences can be improved following post-refinement of partiality. Section IV deals with the explicit simulation of an existing experimental single crystal dataset that was collected with a weakly converging LCLS beam. The subsequent addition of source convergence, or "cross-fire," is simulated for a range of angles in order to evaluate overlap of orders for single and double pattern measurements. Section V simulates and processes a complete probe-pump-probe dataset by the Convergent Beam Method, based on synthetic coordinate-based structure factor amplitudes for a ground state and an intermediate state structure of PYP. Section VI discusses the required physical parameters for X-ray optics and the detector which are under development at the MID station at the European XFEL in order to implement the proposed experimental scheme. Finally, Sec. VII includes discussion of a possible extension of the three-pulse probe-pump-probe geometry to nanocrystals using SFX.

II. CRYSTALLOGRAPHIC DETECTION OF FEMTOSECOND POPULATION TRANSFER REQUIRES HIGH SIGNAL-TO-NOISE

Based on the data analysis of successful pump-probe experiments conducted at synchrotrons, it can be argued that the signal-to-noise ratio of the crystallographic data would need to

be matched or exceeded at XFEL sources in order to develop the ability of detecting a femtosecond transient population. A primary concern is that femtosecond population transfer is intrinsically limited by the photoisomerisation quantum yield, in contrast to nanosecond excitation of protein crystals performed at synchrotrons which may generate yields that can be several times the primary photoisomerisation quantum yield. Experimental approaches to maximize the femtosecond photolysis of protein crystals have been described earlier. For instance, we have reported a femtosecond spectroscopy and (passive) pulse shaping study, which was aimed at characterization and optimization of femtosecond population transfer of the photoactive yellow protein specifically for XFEL experiments.[20] Within the available signal-to-noise of the crystallographic detection, successful femtosecond pump-probe experiments must very likely include such careful pulse shaping approaches. We have shown that photochemical yields may differ by orders of magnitude depending on the details of peak power, second order dispersion, wavelength, pulse duration, and penetration in anisotropic media. A second concern is that the crystallographic data quality can be limited by X-ray source noise at XFELs. For single crystal studies, crystallographic analysis of monochromatic X-ray diffraction data of PYP collected in SASE mode with monochromation indicated that the signal-to-noise ratio of the merged data is dominated by pulse-to-pulse intensity fluctuation and has additional noise contributions from structure in the incident beam intensity and jitter of this structure.[22] By applying the rotation method for single crystal experiments, the resulting signal-to-noise was found to be at least an order of magnitude worse than for typical synchrotron data.[22] From this analysis, it was possible to estimate the resulting crystallographic merging statistics based on the measured pulse intensities during data collection in combination with known average rocking curve profiles. For example, one multi-crystal dataset which merged reflections from 96 rotation images led to a multiplicity of 4.8 and a signal-to-noise ratio of 3.2, which is in agreement with a value that was modeled on the basis of the source noise statistics.[22] This approach shows that the potentially increased stability obtained in self-seeded mode might improve the statistics, but specifically for crystals which have large mosaic spread (thus excluding the photoactive yellow protein). Yet even under such more optimal conditions, it may not be possible to reach the required signal-to-noise levels for a single pump-probe delay within the time-frame of a typical scheduled experiment. An alternative to single crystal studies considers time resolved pump-probe application of SFX, which has been shown to provide sufficient signal-to-noise to detect intermediates when nano-second photolysis is used.[15,16]

III. A SPLIT BEAM PROBE-PUMP-PROBE SCHEME IS PROPOSED IN ORDER TO INTERNALLY REFERENCE THE SOURCE INTENSITY NOISE OF THE XFEL

A focused, non-collinear split-beam geometry is proposed in order to address the issues of (1) pulse-to-pulse intensity fluctuation and (2) partiality of reflections when monochromatic radiation is used. A pulse replica is created with a beam splitter, either by a thin Bragg crystal used as optical splitter with 1:1 ratio between the reflected and transmitted beams or by a Bragg crystal positioned halfway into the beam (geometrical splitter), such as already established for soft X-ray experiments using mirrors at the AMO beamline at LCLS[23] or at FLASH at DESY.[24,25] By introducing a sufficient angle (approximately 0.5°) and delay (>1 ps) between the pulse replicas, it is possible to create a "probe-pump-probe" pulse sequence where diffraction of pumped and unpumped signals are collected at different positions on an area detector (see simulation in Figure 5). As these will be conducted with a stationary crystal, additional focusing of the beams is proposed as the most practical method to address partiality. The three beam probe-pump-probe experiment should hence allow a ratiometric measurement of the photo-induced structure factor differences ΔF.

It is noted that a related approach has been suggested by Fournier and Coppens,[26] which is different however as these authors report the use of photo-induced differences between the same Bragg reflections. Equation (1) defines the photo-induced ratiometric intensity difference for Bragg reflection A

$$\frac{\Delta I_A}{I_A} = \frac{\left[I_A^{PUMPED} - I_A^{UNPUMPED}\right]}{I_A^{UNPUMPED}} \tag{1}$$

whereas the use of an offset angle in a three-pulse probe-pump-probe experiment determines the ratios of Bragg reflections A and B as in Eq. (2) if the offset angle exceeds the mosaic spread. However, this assumes that "full" reflections are being measured

$$\frac{\Delta I_A}{I_B} = \frac{I_A^{PUMPED}}{I_B^{UNPUMPED_{frame1}}} - \frac{I_A^{UNPUMPED}}{I_B^{UNPUMPED_{frame2}}} \tag{2}$$

Here, $I_B^{UNPUMPED}$ is measured twice in a stationary geometry, in two different frames, to serve as an internal reference. For Bragg reflections that are partially measured, the full intensity of reflection A, I_A, full is given by

$$I_{A,full} = \frac{I_{A,partial}}{p_A L_A} \tag{3}$$

where p_A is the partiality and L_A is the Lorentz-polarisation factor, which for the oscillation method corrects for the velocity by which the reciprocal volume traverses the Ewald sphere, in addition to correcting for the polarization of the incident X-rays.[27–29] In the case of a stationary crystal measurement by the Convergent Beam method, which is the proposed geometry for the probe-pump-probe scheme discussed below, the "pseudo" Lorentz factor still contains a $(\sin 2\theta)^{-1}$ geometrical factor, as well as a polarization correction, but in addition includes a source factor "S" which contains the non-uniform source angular distribution including the sources S_0, S_C, and S_1 (Figure 1), taken as[30,31]

$$S = \int_C I(\gamma, \varphi) dC \tag{4}$$

A ratiometric photoinduced difference measurement of partial reflections are thus determined as

$$\frac{\Delta I_A}{I_B} = \frac{p_B L_B}{p_A L_A}\left(\frac{I_{A,partial}^{PUMPED}}{I_{B,partial}^{UNPUMPED_{frame1}}} - \frac{I_{A,partial}^{UNPUMPED}}{I_{B,partial}^{UNPUMPED_{frame2}}}\right) \tag{5}$$

The principal motivation for selecting the convergent beam method is to reduce differences in partiality of I_A and I_B in both unpumped and pumped frames. Both shot-to-shot source jitter of the spatial overlap of the non-collinear X-ray beams as well as shock-induced reorientation ("twitching") of the crystal are expected to lead to large errors of the measured quantities in Eqs. (2) and (5) if non-converging beams are used. An experimental demonstration of such sensitivity was obtained at LCLS by repeated stationary measurements which showed considerable variation of the shot-to-shot intensity ratios of Bragg peaks.[22]

Thus, increasing the angle of convergence to be bigger than the mosaic spread will lead to an effective integration over the rocking curve and many reflections will be measured as "fulls." In order to apply the convergent beam method to a probe-pump-probe experiment, post-refinement of partiality is needed.[32] Under such conditions and with a ratiometric detection of the simultaneously measured unpumped and pumped reflections, noise contributions from the intensity fluctuations are significantly reduced. This is also true if the experiments are conducted in a stroboscopic manner, i.e., summing over several pump-probe cycles. Thus, in the absence of other errors, the resulting data quality of photo-induced difference measurements becomes limited by the dynamic range of the detector and the accuracy of post-refinement of partiality. In SASE mode at 9 keV and employing a Si(111) monochromator reflection, the resulting intensity noise was measured and characterized by a distribution having an $I/\sigma I$ value of 1.2.[22] This value would represent the accuracy by which differences are measured in the

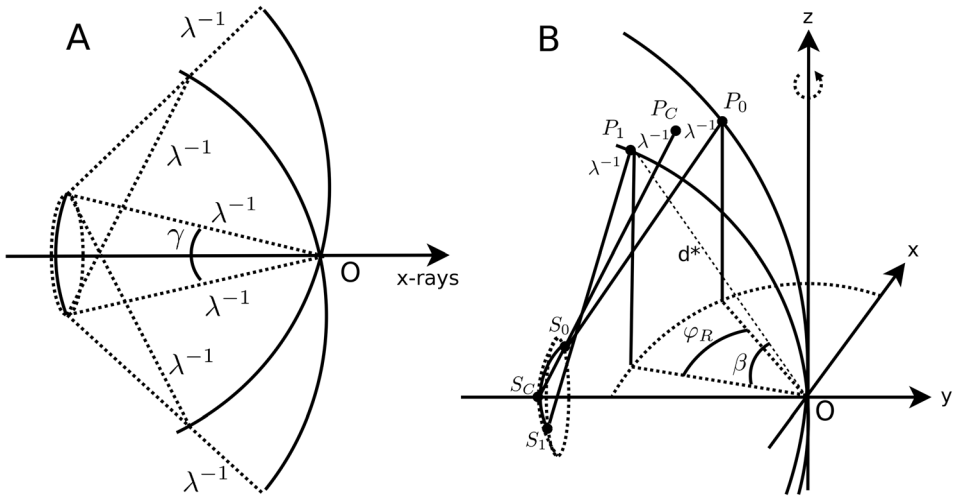

FIG. 1. Convergent Beam Method geometry. (a) Ewald construction for a nest of Ewald spheres for blind region conditions in the presence of beam convergence with angle γ (exaggerated). Bragg conditions are satisfied for source centres that lie on a spherical cap with maximal angle γ. (b) Ewald construction representation of the reflecting range φ_R for rotation around the z-axis, for the limiting range of reciprocal lattice points P_0, P_C, and P_1. The corresponding sources S_0, S_C, and S_1 are found on a line on the source spherical cap.

absence of the internal referencing that is proposed here. Considering, for example, the dynamic range of a MAR165 detector, which is 16 bit, requiring measurements up to 6 σ intensity range, the mean distribution would be measured at an effective dynamic range of approximately 14 bit. Since different Bragg reflections are measured in each image (Eqs. (2) and (5)), a ratiometric dataset will be constructed after merging of multiple ratiometric observations, where the final merged ΔF values are determined with accuracies depending on the multiplicity as well as the number of individual Bragg peak ratios that are included.

The convergent beam method and geometry for macromolecular X-ray crystallography has been described earlier for incoherent sources[30,31] and coherent sources.[33] It has been pointed out that for beam diameters larger than the unit cell and smaller than the crystal, the source coherence should have no contribution to the diffraction pattern.[33] While the geometry is well known for the convergent beam method, there are different approaches to calculating partiality in the literature. It is additionally useful to briefly review the contributions of beam convergence (or "cross-fire") γ, mosaic spread η, and spectral dispersion $\delta\lambda/\lambda$.

For a convergent beam with focusing angle γ and focal point on the reciprocal origin where the nest of Ewald spheres cross over (Figure 1(a)), the point sources (S) for reciprocal lattice points (P) are located in a line on the source spherical cap (Figure 1(b)). Therefore, in the presence of a focusing angle γ diffraction spots become elongated on the area detector, and may result in overlapping of orders for large values of γ.[30,31,33,34] The Bragg condition is met within the two limiting conditions as given by the following equation:[30,31]

$$\cos\left(\beta+\frac{\gamma}{2}\right) \le \frac{\lambda d^*}{2} \le \cos\left(\beta-\frac{\gamma}{2}\right) \tag{6}$$

where γ is the maximal convergence angle, $d^* = |OP|$, $\sin\beta = P_Z/d^*$, and λ is the wavelength. It has been shown (Refs. 27–29, 32, 35–37, and references therein) that the contributions of γ and η to the Bragg condition equations are equivalent and hence can be summed to find the reciprocal lattice volume radius as

$$\Omega = \gamma + \eta \tag{7}$$

Including the spectral dispersion $\delta\lambda/\lambda$ a Ω_δ has been defined as[37,38]

$$\Omega_\delta = \gamma + \eta + \frac{\delta\lambda}{\lambda}\tan\theta \tag{8}$$

where θ is the Bragg angle. The reflection range (Figure 1(b)) is approximated by Greenhough and Helliwell as[37]

$$\varphi_R \cong L\left(\Omega d^* \cos\theta + \frac{\delta\lambda}{\lambda} d^* \sin\theta\right) \tag{9}$$

The partiality is generally obtained from calculation of the intersection of the Ewald spheres with the reciprocal lattice point volume. In the case of still images collected at XFEL's with nano-crystals and a non-divergent source, partiality is analysed to calculate both the minimal and maximal radius for the Ewald sphere volume that intersects the reciprocal sphere volume, as implemented in the CrystFEL code for SFX data reduction.[32] Subsequent post-refinement of many partial observations improves the estimate of the full intensity. In the case of a convergent beam method where the convergence angle exceeds the average mosaic spread and many, but not all, reflections are recorded as "fulls." Subsequent calculation of partiality may be done by retrieving the outside and inside conditions of the reciprocal sphere volume, analogous to the rotation method. The partiality p is shown to be well approximated by[37]

$$p \cong \frac{1}{2}\left(q_\varphi + 3q_\varphi^2 - 2q_\varphi^3\right) \tag{10}$$

where the inside condition "$q_{\varphi 1}$" and outside condition "$q_{\varphi 0}$" are the fractions of paths travelled by the reciprocal lattice point P, and are given by[27,28,37]

$$q_{\varphi 1} = \frac{1}{2}\left(1 + \frac{(\beta - \theta)}{\Omega_\delta/2}\right) \tag{11}$$

$$q_{\varphi 0} = \frac{1}{2}\left(1 - \frac{(\beta - \theta)}{\Omega_\delta/2}\right) \tag{12}$$

It should be noted that a recent simulation study of weakly converging conditions, γ up to 2.5 mrad ($\sim$0.14°) was reported for SFX.[33,39] Although the value of the mosaic spread was not discussed, the resulting data processing and post refinement indeed showed both a considerable increase in the values of partiality as well as a significant improvement of the (SFX-specific) "R_{split}" value.[33,39] This also confirms that data reduction including post-refinement of partiality should yield better measurements of (2) and (5) in the case of the convergent beam method.

IV. SIMULATION OF MONOCHROMATIC X-RAY DIFFRACTION OF $P6_3$ CRYSTALS OF PYP WITH A WEAKLY CONVERGING XFEL BEAM REPLICATING EXPERIMENTAL FRAMES AND SUBSEQUENT SIMULATION OF ADDITIONAL BEAM FOCUSING

We now consider which angle of convergence could be used in order not to cause too much lengthening of the Bragg spots and avoid overlapping orders in single and double patterns. Here, ray tracing simulations first replicate an experimental monochromatic XFEL dataset which was previously reported.[22] The dataset in question originate from a single crystal study of PYP crystals conducted at the XPP station at LCLS, April 2012. The experimental diffraction images were taken under conditions of very weak convergence of the XFEL beam (0.007°) and under conditions of low absorbed dose. Both still images and rotation images were analysed.[22] The simulations were done using the program SIM_MX from Kay Diederichs[40] and use input parameters from experimental conditions including the mosaic spread taken from rocking curve measurements.[22] The simulations were found to replicate the spot sizes and their separations well. Next, the effect of increasing beam focusing, or convergence, on the simulated spot sizes and their lengthening is explored, which takes into account a realistic point spread

function in the ray tracing simulations. We note that it is insufficient to consider only the overlap of orders within a single diffraction pattern for which analytical expression can be written, because two patterns are collected on an area detector, as simulated and described in Sec. V.

The experimental conditions were as follows: sample-detector distance (59.1 mm), detector parameters (detector radius 165 mm; 0.079 mm pixel size, 2048 × 2048 pixels, MAR165 detector, MarResearch), wavelength (1.3099 Å), bandwidth ($\Delta E/E = 1.6 \times 10^{-4}$), and unit cell parameters (66.9 Å, 66.9 Å, 40.8 Å, 90°, 90°, 120°, $P6_3$). Figure 2 shows on the left an experimental diffraction pattern collected using the rotation method with a 0.1° oscillation, including an average of approximately 200 Bragg spots per image, extending to 1.5 Å resolution at the detector edge. For the rocking curve measurements, fifty X-ray pulses were used for each image, having up to five pulses probing the average rocking curve of each reflection, and it was estimated that the I/σI value of a single Bragg reflection was 1.47 under these conditions.[22] In order to obtain an average value for the mosaic spread measured under such conditions of significant noise, a series of individually measured rocking curves of a PYP crystal were obtained, which provided a distribution between 0.01° and 0.07° with an average value of 0.04° (FWHM).

The first objective was to determine simulation parameter values in order to replicate the experimental diffraction patterns in detail, specifically replicating the spot dimensions and separations. For the ground state, amplitudes were calculated using sfall[36,41] from the coordinates taken from 2PHY.pdb,[1] using a resolution cut-off at 1.5 Å. Reflections were expanded to space-group P1 using sftools[36] and expanded to full sphere including Friedel pairs using a custom program.[40] It was found that in order to simulate the same Bragg spots from identically indexed orientations present on a single frame required using a simulated rotation image with a 0.2° oscillation rather than the experimental 0.1° oscillation. Similarly, we found that replicating the same Bragg peaks by simulations of stationary diffraction patterns collected under conditions of weak beam convergence required specifying a small oscillation in addition, typically 0.1°. This is potentially due to the simple mosaic block model used by SIM_MX taking as input an average and isotropic value for the standard deviation of the mosaic spread. Experimentally, a mosaic spread is observed that is anisotropic and includes line defects.[22] Therefore, all presented simulations below included an oscillation range of at least 0.1°, also when stationary patterns were calculated.

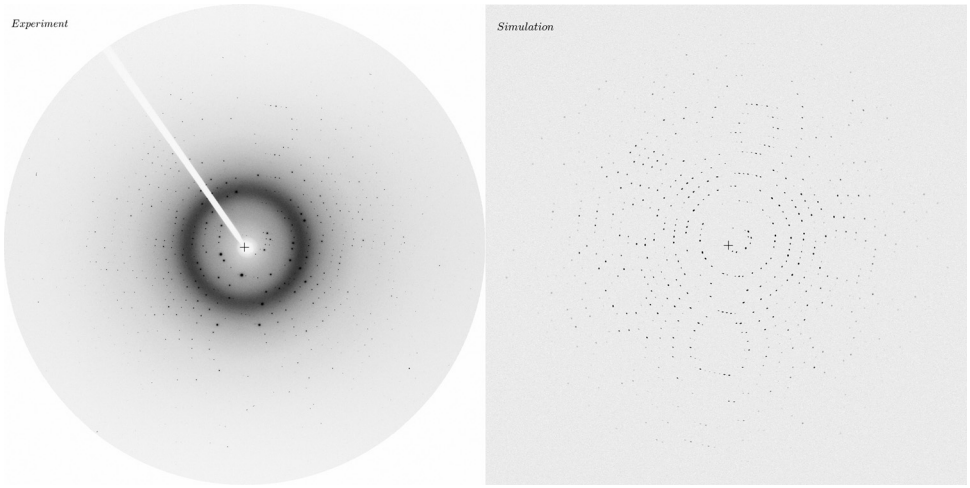

FIG. 2. Left: Experimental X-ray diffraction pattern of a PYP crystal using the rotation method over a 0.1° oscillation. The edge of the detector corresponds to 1.5 Å resolution. Right: Simulation of X-ray diffraction in the same indexed orientation and geometric parameters as the experimental image. A beam convergence more than 10 times greater than the experimental conditions (0.1°), also giving larger spot sizes, is used in order to emphasize the close correspondence between experimental and simulated patterns. The realistic ray tracing simulations were done with the following parameters: Unit cell 66.37 Å, 66.37 Å, 40.67 Å, 90°, 90°, 120° $P6_3$. Mosaic spread 0.04° (isotropic). Beam divergence 0.1°, $\Delta E/E = 1.6 \times 10^{-4}$, wavelength 1.3099 Å, and detector-sample distance 51.9 mm. Detector: Mar165, 165 mm diameter, 2048 × 2048 pixels. Simulated resolution range of 1000–1.5 Å. The simulation was performed with the SIM_MX program.[40]

Specific simulation parameters used were root mean square deviation for the unit cell dimensions 0.04 Å, 0.04 Å, and 0.04 Å (for a, b, and c), and standard deviation for the average isotropic mosaic spread 0.04°. Cell dimensions, wavelength, band-width, and detector distance and geometry were as used in the experiment. In addition, simulations for large crystals result in larger spots distributed over four pixels accounting for a finite size beam and a finite size crystal. It is noted that the experimentally determined average value of FWHM = 0.04°, which corresponds to a standard deviation of 0.017°, may not fully explain the need for a larger oscillation range in the simulations in order to replicate the Bragg spots. However, the primary aim to first reproduce the experimental images by simulation in terms of replicating spot positions, sizes, and separations, is achieved with only minor differences from actual physical values. While the positions and dimensions are reproduced very well by the simulations, there are clear differences in the relative spot intensities compared with experiments (compare Figures 3(a) and 3(b)). The intensity noise of the LCLS contributes to these differences. In addition, since the simulated data are computed from coordinates deposited in the PDB database, systematic errors also lead to differences between experimental and simulated intensities (Figure 3, Table I).

For Figure 2, the simulation used a 0.1° beam divergence in order to increase the spot size facilitating a visual comparison of the reproduced pattern with the experimental image.

It is seen in Figures 3(a) and 3(b) that the experimental spot size (with a convergence angle of 0.007°) corresponds closely to a simulated image with divergence angle of 0.01°. The intensity traces shown below Figures 3(a) and 3(b) illustrate the experimental images and the simulated ones, respectively, and have a typical cross section of three pixels in this geometry. It is noted that this average spot size was representative for all resolution ranges and Figure 3(a) shows the intermediate resolution range as an example. The effective point spread function arising from the ray-tracing simulation parameters therefore resulted in a realistic reproduction of the experimental data, which then allows simulation of additional focusing. Hence, subsequent simulations varied the value of the convergence angle from 0.01° to 0.25° (in both directions). The simulated patterns highlight the resulting increase in spot size and lengthening that will result in overlapping. The overlaps will become more prevalent at larger focusing angles if a second set of spots from an identical unit cell is present (probe-pump-probe geometry), of course depending on the separation of their origins.

V. SIMULATIONS AND PROCESSING OF A SPLIT BEAM "PROBE-PUMP-PROBE" DATASET

A simulated "probe-pump-probe" dataset containing two patterns is now generated using SIM_MX on the basis of coordinates for the ground state (2PHY.pdb)[1] and a photo-intermediate determined using the pump-probe Laue method (3UME.pdb).[42] Coordinate based structure factor amplitudes were thus used to create the overlaid diffraction patterns, which are subsequently processed to retrieve the individual data from the mixed patterns. This demonstration shows that realistic parameters for the proposed multi-beam experiment will enable femtosecond time resolved X-ray crystallography of protein single crystals in this manner (Eqs. (2) and (5)). From the simulated spot sizes, a value of 0.12° for the convergence angle was chosen in order to simulate the "probe-pump-probe" dataset. This value exceeds the average mosaic spread of PYP crystals and hence applies the convergent beam method effectively, but minimizes the resulting spot lengthening. In order to spatially separate the "unpumped" and "pumped" patterns on the area detector, an offset angle of 0.5° is chosen which allows sufficient spot separation. In the chosen geometry, this results in a shift of the direct beam center by 0.516 mm, corresponding to 6.5 pixels. As shown in Figure 4, the introduced offset angle is in the vertical plane orthogonal to the goniometer rotation axis. In this way, ratiometric measurements can be made twice for each reflection if single crystals are rotated between stationary CBM measurements: once for the "unpumped" measurement and once for the "pumped," but relative to different reflections (Eqs. (2) and (5)). This will allow an improved data correlation

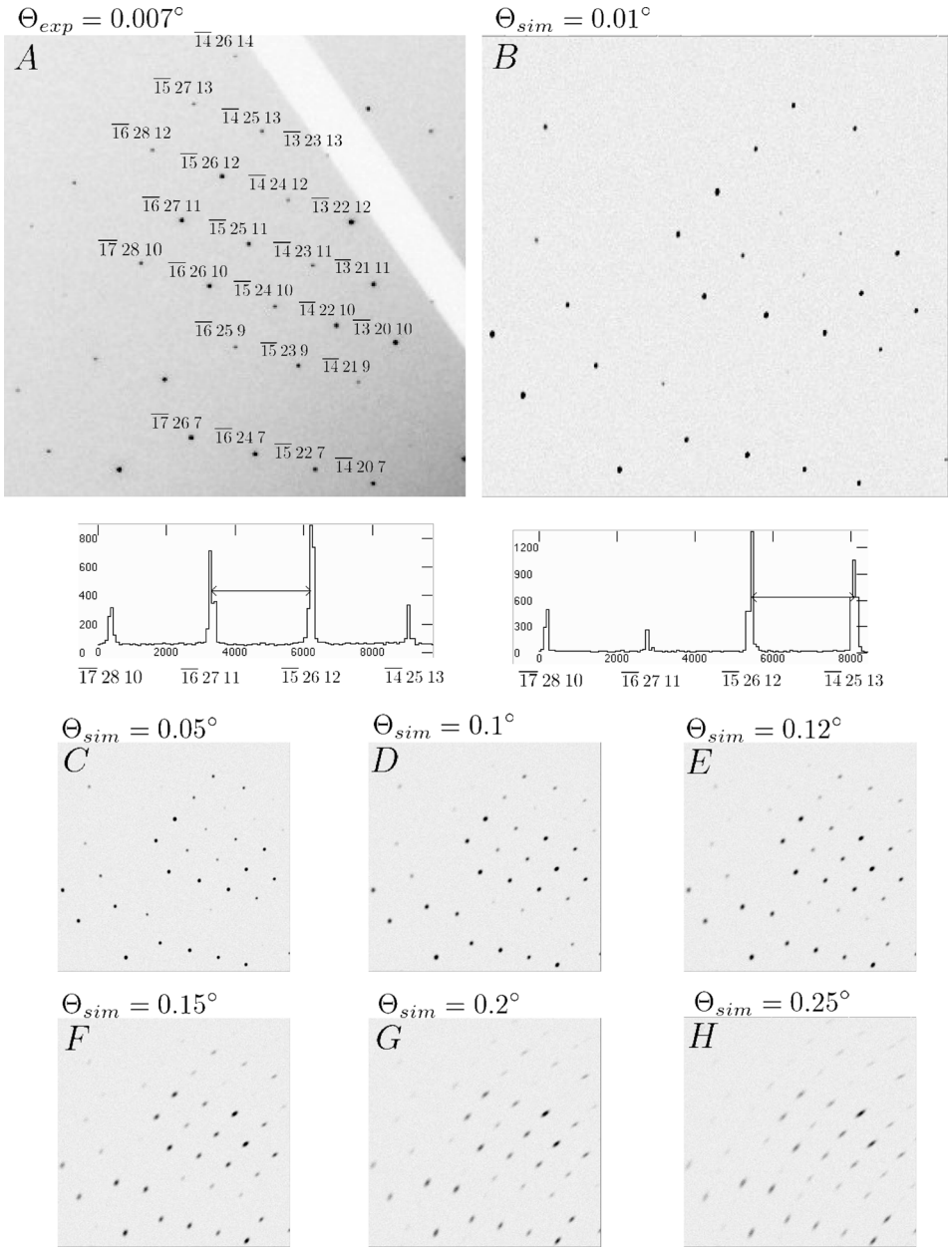

FIG. 3. A comparison of experimental (a) and simulated (b)–(h) Bragg spot dimensions. (a) An intermediate resolution region shown for the same pattern seen in Figure 2, with Miller indices included. The experimental convergence angle was 0.007°. A trace for the intensities of the (−17, 28, 10), (−16, 27, 11), (−15, 26, 12), and (−14, 25, 13) reflections is shown below the zoomed region below the experimental (a) and simulated (b) patterns. (b) Corresponding region of the simulated diffraction pattern, together with an intensity trace of the same Bragg spots shown in (a). (c)–(h) Corresponding simulations with 0.05°, 0.1°, 0.12°, 0.15°, 0.2°, and 0.25° beam convergence.

for the ratiometric datasets, additionally taking advantage of the short time delay between collecting the two measurements thus ameliorating radiation and laser induced damage as well.

A "pumped" dataset was generated from coordinates for a time-resolved intermediate with an isomerised chromophore and various structural differences in protein and solvent conformation, taken from 3UME pdb.[42] It is noted that this "pB" intermediate of PYP is developed 200 μs after excitation, and therefore in practice not suitable for a split-and-delay experiment proposed here. The intermediate was selected as a proof-of-principle to demonstrate that, using the coordinates of a well refined time resolved intermediate of PYP, the ΔF's can subsequently

TABLE I. Data processing of the individual simulated data-sets (columns 2 and 3) and the merged probe-pump-probe dataset (columns 4 and 5).

Dataset	2PHY-sim	3UME-sim	2PHY-probe-pump-probe	3UME-probe-pump-probe
Refined cell	66.36, 66.36, 40.66, 90, 90, 120 $P6_3$	66.37, 66.37, 40.67, 90, 90, 120 $P6_3$	66.35, 66.35, 40.65, 90, 90, 120 $P6_3$	66.37, 66.37, 40.66, 90, 90, 120 $P6_3$
Refined beam center and distance	1024.02, 1023.96, 59.088	1024.04, 1030.97, 59.091	1023.98, 1023.98, 59.081	1024.04, 1030.97, 59.091
Refined incident beam direction (X,Y,Z)	-2.9×10^{-5}, 4.6×10^{-5}, 1	-7.1×10^{-5}, 0.0087, 0.9996	3.5×10^{-5}, -4.5×10^{-5}, 1	2.8×10^{-5}, 0.0092, 0.9996
No. spots/unique	173 017/16 398	177 771/16 382	160 186/16 393	169 732/16 415
Completeness	99.9%/99.9%	99.9%/99.9%	99.7%/99.7%	99.9%/99.9%
I/σI	145.3/40.9	218.8/51.6	61.0/23.8	101.6/38.5
R-merge[a]	1.2%/5.7%	0.9%/4.6%	2.5%/8.8%	1.6%/6.0%
R-meas[b]	1.3%/5.9%	1.0%/4.9%	2.6%/9.3%	1.7%/6.3%
R-cryst	1.7%	1.1%	2.1%	0.9%
R-free	1.6%	1.1%	2.0%	0.9%

[a] $R_{merge}(I) = \sum_{hkl}\sum_{i}|I_i(hkl) - \langle I(hkl)\rangle| \Big/ \sum_{hkl}\sum_{i} I_i(hkl)$.

[b] $R_{meas}(I) = \sum_{hkl}\sum_{i}^{n}\left(\frac{n}{n-1}\right)^{1/2}|I_i(hkl) - \langle I(hkl)\rangle| \Big/ \sum_{hkl}\sum_{i} I_i(hkl)$.

be retrieved from processing the synthetic probe-pump-probe dataset. The "pumped" dataset (3UME) was generated in the identical indexed orientation as the "unpumped" dataset (2PHY), additionally specifying a 0.5° angle of incidence for the "pumped" simulation. Since the indexed orientation shown in Figure 2 had only a very small angle between the crystallographic c-axis and the rotation axis, a different indexed orientation was chosen which had a larger angular offset. A full 180° dataset was then generated with 0.2° rotation steps, having intensities on the same scale for the 2PHY and 3UME datasets. 0.2° rotation images were chosen

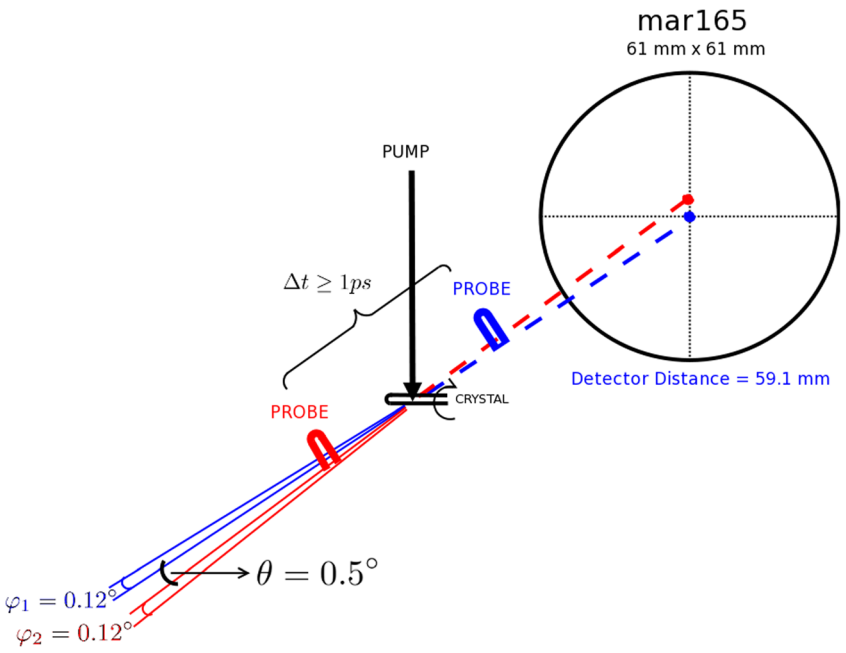

FIG. 4. Two-beam geometry used for the X-ray ray-tracing simulations. An angle of 0.5° is introduced between probe beams with an additional time delay of >1 ps allowing for a stretched or shaped optical pulse in between the two X-ray pulses. Both beams are in a plane orthogonal to the goniometer rotation axis, and both have a 0.12° convergence angle.

for this simulation according to the discussion above and with regard to the number of spots it would correspond to two, or more, subsequent stationary CBM diffraction patterns measured in one frame. One frame of the full probe-pump-probe simulation is shown in Figure 5.

It was found that even for the increased number of spots in each frame relative to a single stationary CBM exposure, spot overlap was not problematic. This is demonstrated by the data in Table I. The individual datasets "2PHY" and "3UME" were individually integrated, scaled, and merged (Table I, columns 2 and 3) before the images were added together. To create the full probe-pump-probe dataset, 900 pumped and unpumped images were summed using the merge2cbf program from the XDS crystallography software suite.[35] The two lattices were then separately integrated from the synthetic dataset after indexing and geometry refinement (Table I, columns 4 and 5), using XDS.[35]

The integration of the synthetic dataset did result in fewer observations (Table II, columns 4 and 5) than the individually processed datasets (Table I, columns 2 and 3), thus indicating some spot rejection due to overlaps or too small spot separations. The geometrical parameters, however, correspond very closely with the individually processed data (Table I). The I/σI values for the merged and scaled data are approximately half that of the individual datasets, which is likely caused by the amplitude normalization performed by merge2cbf. As expected, R-merge, R-meas, R-cryst, and R-free are very small, reflecting mostly the numerical accuracy of the ray traced intensities. More informative though is the correlation between the integrated, merged, and scaled amplitudes for the individual and the synthetic datasets. Figure 6 illustrates that the correlations between the individually processed 2PHY and 3UME datasets and the separated probe-pump-probe datasets is close to unity and is likely within the numerical accuracy of the simulation and processing software. A final validation of the simulation is provided by the fact that chromophore-omit electron density maps show only density for the cis (2PHY) and trans (3UME) conformations, respectively. To illustrate this further, a Fourier difference electron density map is shown for the retrieved ΔF's from the synthetic probe-pump-probe data, applying ground state phase angles (from 2PHY) (Table I, columns 4 and 5, and Figure 7).

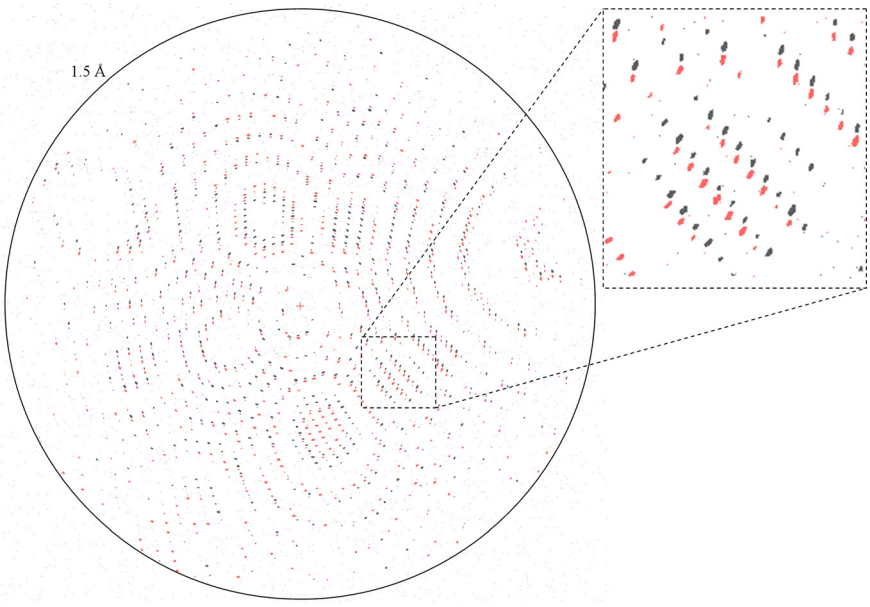

FIG. 5. One frame of the full simulated "probe-pump-probe" dataset on the Mar165 detector. Parameters were the same as used for Figures 3(e) and 4, except for using a different indexed orientation. The resolution extends to 1.5 Å at the edge. Black spots are for the "unpumped" structure generated from the 2PHY PDB coordinates, the red spots are from the "pumped" structure calculated from 3UME. Right: a zoomed region highlights the spot separation achieved by the dual-beam geometry. The angles of convergence for both datasets were 0.12°, and the offset angle between replicas was 0.5°, as in Figure 4.

It should be noted that these simulations did not vary the incident intensity, which would

TABLE II. Proposed parameters for three-beam probe-pump-probe measurements.

	Single crystal application	SFX application	SDL/MID (XFEL.EU)
Convergence angle (both beams)	0.12° (optimized value; 0.15° max, no convergence potentially tolerable)	0–0.12° (non-convergent beam acceptable for high-throughput SFX measurement)	Up to ∼0.12°, depending on the focusing optics
Angle between beams	0.5° (based on MAR165 detector, and experimental parameters used during XPP44112). Control of the value would allow big and small unit cells (0.1°–0.8° range)	0.5°	Up to ∼0.6°, depending on the mirror material chosen (Si/Pt)
Time delay between pulses	>1 ps. Ideally controlled 1–10 ps	>1 ps	Design specs: 0–800 ps +/− 3 fs
Bandwidth	1.6 eV	1.6 eV	$\sim 6 \times 10^{-5}$ (0.3–0.6 eV) (Si 220 reflection)
Photon energy	9–9.5 keV	9–9.5 keV	5–10 keV (adjustable)
Photons/pulse	$> 10^{10}$–10^{11} each beam	10^{7}–10^{10} each beam (non-destructive)	10^{8}–10^{11} per pulse, adjustable, depending on SASE/seeding
Source stability	Not intrinsically required	Not intrinsically required	Desirable
Repetition rate	Up to full machine rate (LCLS = 120 Hz). For PYP: 2 Hz	Detector limited	3.5 kHz, detector limited
Spot size on target	40 μm, round or up to 150 × 40 μm aperture	∼1–10 μm	<1–100 μm, variable
Overlap between beams on target	Better than 5 μm precision	Better than 100 nm precision	Design specs: better than 80% overlap area

be expected to affect the effective dynamic range of the numerical accuracy. Rather, it is shown here that realistic beam parameters can be chosen (see details about the split-and-delay instrument in Sec. VI) that, in addition to focusing provided by suitable X-ray optics, will result in spatially separated diffraction patterns which can be individually integrated. An actual probe-pump-probe experiment could be either single stationary CBM images or alternatively rotate between measurements and sum several stationary CBM experiments (in the case that the X-ray

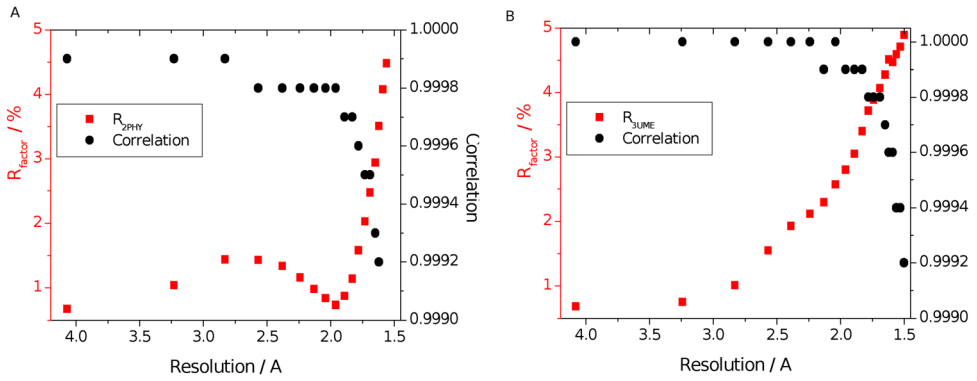

FIG. 6. Cross correlation and R-factor for the individually processed simulated datasets 2PHY (a) and 3UME (b) and the synthetic probe-pump-probe dataset. (a) Columns 2 and 4 of Table I. (b) Columns 3 and 5 of Table I. Left y-axis (red squares) are the R-factors, right y-axis (black circles) are the degree of correlation.

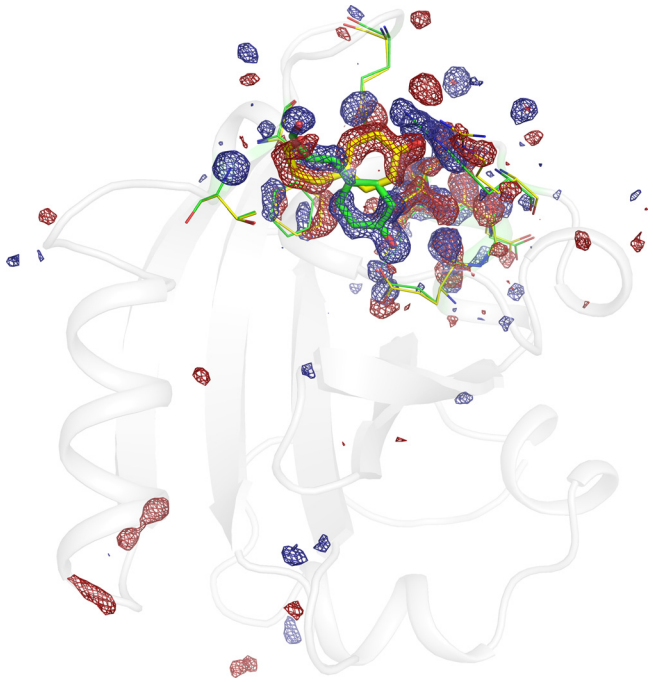

FIG. 7. Retrieved F_{3UME} minus F_{2PHY} electron density difference map with applying phase angles calculated from 2PHY coordinates. Red contours are at $-4\ \sigma$ level, blue contours are at $4\ \sigma$ level. Coordinates for the most significant differences are shown (yellow: 2PHY, green: 3UME). The coumaric acid chromophore is represented with thick bonds in *cis* and *trans* conformations.

repetition rate exceeds the detector frame rate; Table II) to collect an extended range of reciprocal space on a single frame.

VI. SIMULATION OF PROBE-PUMP-PROBE X-RAY DIFFRACTION AT THE EUROPEAN XFEL AND PHYSICAL PARAMETERS FOR A SINGLE ENERGY SPLIT AND DELAY INSTRUMENT

The Materials Imaging and Dynamics (MID) experimental station[43] being constructed at the European XFEL (XFEL.EU) combines a state-of-the-art hard X-ray split and delay unit (developed in collaboration with the Technical University of Berlin) with a custom made high frame rate area detector (AGIPD).[44–46] The AGIPD has been designed to operate at 4.5 MHz frame rate in order to record an image for each X-ray pulse. The XFEL.EU will generate 10 macropulses/s each of them containing 2700 pulses with 220 ns spacing (4.5 MHz), thus allowing a maximum of 27 000 frames/s to be used by the experiments but AGIPD can only record about 350 images per macropulse due to limitations in internal storage. The AGIPD consists of 4 pixelated tiles that can be moved individually, e.g., to accommodate a hole or a slit in the middle through which the direct beam is transmitted without damage to the detector. In total, the detector has 1M pixels each of $200 \times 200\ \mu m^2$ size, a full well capacity of 34 Me^-, and a dynamical range of about 100 k. This will allow detection of more than 10^4 photons/pixel/pulse at 9 keV and the rms noise is well within the limits of single-photon sensitivity. For comparison, the full well depth and dynamic range of a MAR 165 detector are 400 ke^- and 45 000, respectively, and like for any other commercially available area detector, it cannot operate at 4.5 MHz frame rate. Taking 9 keV X-ray energy and a sample-detector distance of 200 mm as simulation parameters, the diffraction in the corners of the detector in fully open configuration amounts to 2.0 Å resolution, see simulation in Figure 8. However, the simulation of a synthetic dataset for this geometry (performed using $\Delta E/E = 1.68 \times 10^{-3}$ to compare with results in Sec. V, but noting that the SDL in Figure 9 will deliver $\Delta E/E = 6.1 \times 10^{-5}$) had an effective resolution of 2.5 Å, with only very few observations contributing to higher resolution.

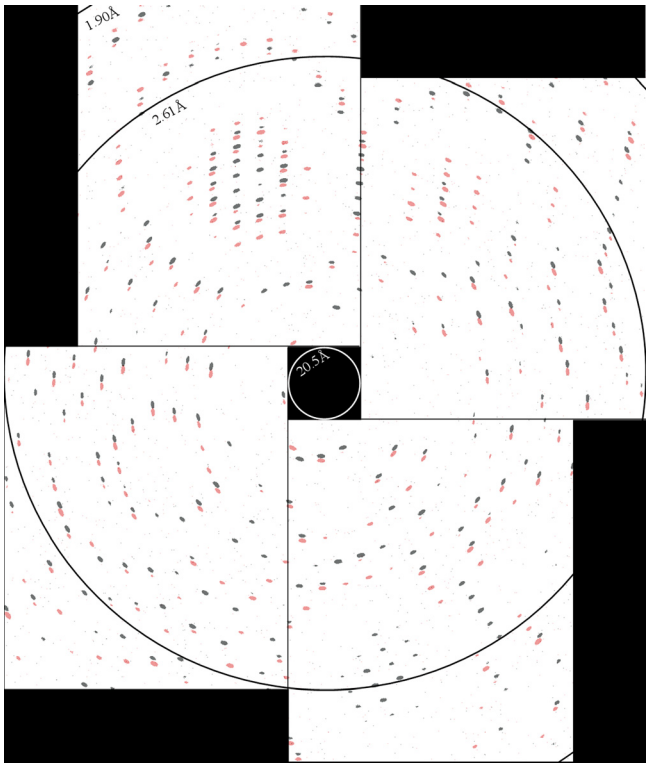

FIG. 8. Simulation of probe-pump-probe diffraction for the open conformation of the AGIPD that will be the standard detector operating at the MID station at the European XFEL. A variable hole in the middle allows the beam transmitted through the sample to pass, which additionally includes loss of diffraction (below 20.5 Å resolution in the simulation performed here). Each of the four quadrants has 512 × 512 pixels organized in an assembly of four modules. The simulation parameters were mosaic spread 0.04°, convergence 0.12°, $\Delta E/E = 1.68 \times 10^{-3}$, wavelength 1.38 Å, and detector distance 200 mm. A 0.4° angle separates the unpumped (black) and pumped (red) diffraction patterns.

A schematic drawing of the principle behind a crystal based hard X-ray split and delay line (SDL) for MID is shown in Figure 9.[43,47–49] First, the beam is passed through a high-heatload cryo-cooled crystal monochromator to reach an energy bandwidth similar to the SDL acceptance. Alternatively, monochromatisation may be obtained by tailoring the SASE process which in the hard X-ray range can be achieved by self-seeding, as previously predicted and demonstrated.[50,51] The beam splitter crystal is marked by "1" and can be either a geometrical splitter

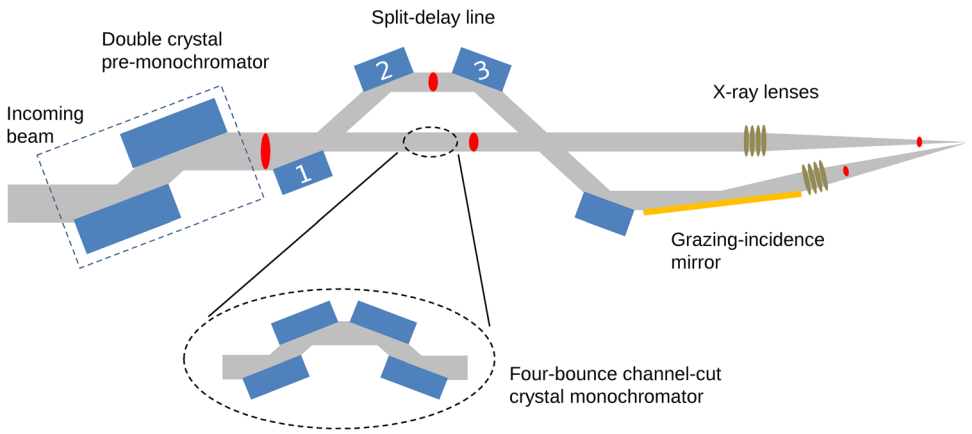

FIG. 9. Schematic of an X-ray split and delay line delivering the time-delayed pulse replicas to the sample with both focusing and off-set angles as in Table II.

as drawn in Figure 9, or a thin crystal operating in symmetric Bragg reflection geometry with equal intensities of the diffracted and the forward scattered beams. It has been discussed that the Bragg geometry results in replica pulses with conserved temporal and spatial structures.[52]

The performance of the thin crystal beam splitter, crystal "1," is the most critical component for successful implementation of a probe-pump-probe measurement. Primarily, the stability of the ratio of transmitted and diffracted pulse intensities will determine the signal-to-noise of the photo-induced ΔF measurement if it exceeds the detector-limited noise. Recently, improved fabrication of thin Si crystals were reported which performed with uniform wavefront ($<\lambda/50$) and low spatial intensity variations ($<5\%$).[52] Lack of thickness uniformity and poor mechanical and temporal stability degrade the performance of the beam splitter when illuminated with intense femtosecond X-ray beams.[43] In the presence of shot-to-shot variations of pointing, mode structure, intensity, temperature, and possibly also remaining spectral fine structure after the monochromator, or from self-seeding, the ratios of transmitted and diffracted beams will be altered as a result of the instabilities in acceptance conditions. If the SDL with a thin optical beam splitter crystal proves to be insufficiently stable, another strategy is to use a geometrical beamsplitter with a thicker perfect Si crystal that is driven halfway into the beam from below. This is actually the situation drawn in Figure 9.

The crystals marked "2" and "3" are positioned to control the beam delay and the beam is sent back to be parallel with the directly transmitted beam, but vertically displaced by an amount that later allows introducing an angular offset. At this moment, the delayed beam has experienced four Bragg reflections while the direct beam has gone straight through. This could create an asymmetry in the spectral purity and hence a four-bounce crystal arrangement is introduced in the direct beam (lower beam path), as indicated in Figure 9. This will also allow compensating the temporal offset between the two beams and, if desired, a temporal overlap ($\Delta t = 0$) can be achieved by lowering crystals 1 and 2. Finally, an X-ray mirror used at gracing angle incidence is reflecting the delayed beam upwards to overlap with the direct beam at the sample position. The angular offset between the two beams is given by two times the incidence angle on the mirror. In order to have 100% reflectivity, it is necessary to operate at or below the critical angle of total external reflection α_C which is 0.20° (0.54°) for a Si (Pt) mirror at 9 keV. Hence, the maximum angular offset can be varied from 0.4° to ∼0.6° depending on the mirror coating and geometrical constraints. The angular convergence of the beams can for instance be achieved by focusing with compound refractive lenses (CRL) made in beryllium. They have the advantage of being in-line optics and hence provide a minimum of disturbance to the complex SDL beam geometry. The angular convergence is then given as two times the numerical aperture (NA) and for CRLs the NA in radians is approximately $2*\sqrt{(\delta/(f*\mu))}$, where $\delta = 1 - n$ with n as the refractive index of X-rays, f is the focal length, and $1/\mu$ is the X-ray attenuation length in beryllium. For 9 keV, one finds NA ∼ 0.06° for f = 100 mm and hence the value used in the simulations for the convergence angle (0.12°) is within reach. Obviously, both beams will need a CRL lens unit and with a focal length of only 100 mm special lens designs are required to accommodate them in the available space in the vertical direction. Alternatively, the focal length can be longer (0.5 m) but with an unavoidable reduction in numerical aperture and hence in angular convergence (∼0.06°).

VII. POTENTIAL FOR A SFX APPLICATION OF THE SPLIT BEAM PROBE-PUMP-PROBE GEOMETRY

A SFX application of the proposed probe-pump-probe geometry would need to use the highest possible pulse intensities that still allow a second X-ray diffraction measurement. For both single crystal and SFX applications, the absorbed dose will need to be significantly below the ∼20 MGy level (known as the "Henderson limit").[17,53,54] However, the tolerated absorbed dose from a single pulse may be higher for SFX than for single crystal applications. While single crystal studies would include multiple pump-probe cycles for each crystal volume over a period of seconds or minutes, in the SFX case only two probes would occur with only picosecond or nanosecond delays. Because of the smaller number of pulses and the shorter time

elapsing between the pulses, SFX experiments may potentially allow a higher absorbed dose for each pulse. There are two considerations for evaluating upper limits for the absorbed dose. First, even a limited level of radiation damage may prevent the successful measurement of photo-induced ΔF. Second, the dose rate may become limiting and will result in explosion of protein crystals when the ablation limit is reached.[17]

Because of the background of radiation damage occurring during repeated stroboscopic pump-probe measurements of the same crystal volume, the ability to detect photo-induced differences can become compromised. Typically, time resolved protein X-ray crystallography data are collected at synchrotron stations at or near room temperature using the Laue technique.[2,55] The 14-ID BioCARS beamline at the Advance Photon Source (Argonne, USA) equipped with two in vacuum undulators in series delivers 4×10^{10} photons per pulse in a $95\,\mu m \times 30\,\mu m$ spot in hybrid mode.[55] Using large, well-ordered crystals, a single 100 ps (pink) X-ray pulse at 12 keV is sufficient to saturate a $80\,\mu m$ pixel of the integrating MAR 165 CCD detector with a low resolution Bragg spot.[55] An estimate of the absorbed dose under such conditions is approximately 20 kGy,[17] which is three orders of magnitude smaller than the ∼20 MGy "Henderson limit," i.e., the theoretical dose that reduces diffraction intensities by a factor of two under cryo-cooled conditions, as derived from cryo-electron microscopy.[53,54] Under conditions of room temperature and including long waiting times between pump-probe cycles which allows radiation damage to further develop, up to a maximum of ∼50 exposures for each fully illuminated crystal volume is characteristically possible, delivering an absorbed dose of ∼1 MGy in typically a few minutes (depending on the repetition rate) before diffraction is degraded. However, the ability to resolve photo-induced ΔFs rapidly reduces after only a few frames under such conditions.

An estimate for the minimum tolerated absorbed dose that allows a second probe using SFX would be ∼20 kGy, which is approximately equivalent to a single synchrotron exposure that saturates the detector. This would imply approximately 7×10^6 incident photons in a $1\,\mu m$ focus. This estimate is based on the reported ∼1 MGy dose determined at 9 keV with 3.5×10^{10} incident photons in a $10 \times 10\,\mu m$ spot for micron sized lysozyme crystals,[12] and takes into account the reported absorption length of $1/\mu = 308\,\mu m$.[17] Although Bragg photons may then only be weakly resolved at high resolution even with single photon detection sensitivity, the high frame rate of the European XFEL may still allow successful and sensitive measurement of probe-pump-probe data under such conditions. Certainly, a probe-probe "dark" measurement would also establish a background for radiation induced differences due to changes in atomic cross section, ionization induced displacement, and loss of order. In addition, at increased pulse intensities, the experiment could be conducted in a time-resolved X-ray pump, X-ray probe manner.

It has been established that XFEL experiments closely matching the above mentioned synchrotron geometry and absorbed dose, allow repeated measurements of the same crystal volume and display a rate of radiation damage that also resembles that seen under picosecond illumination at synchrotrons.[22] Measurements that use large crystals (typical dimensions of $40 \times 40 \times 400\ \mu m$), and use illumination with a defocused and attenuated beam from LCLS allow many frames (>60 frames with 5 X-ray exposures/frame) to be collected on the same crystal volume using the full dynamic range of the MAR 165 detector.[22] In contrast, large crystals that were exposed to the full flux of LCLS without attenuation caused full ablation of the exposed crystal volume and shock induced disorder of the remaining (not illuminated) sample volume.[22]

Detailed studies have shown that with intense XFEL pulses the femtosecond pulse duration "out-runs" radiation damage, and diffraction becomes "self-gated."[12,14,17,18] It was estimated that for a $1\,\mu m^3$ protein crystal volume, which contains approximately 10^{11} atoms, 2.5×10^8 ionisation events occur and 50 000 photons are scattered, at 6 keV and 10^{12} photons μm^{-2}.[17] Recent high resolution SFX of lysozyme microcrystals reported the statistics, flux, dose, and dose rate for both 5 fs and 40 fs bunch duration.[12] For the 5 fs dataset, 3.5×10^{10} photons with 9 keV energy were incident on each crystal in a $10 \times 10\,\mu m$ spot, delivering a dose of 2.9 MGy.[12] The resolution limit of this data, 1.9 Å, was comparable to synchrotron datasets, thus

providing sufficient photon counting statistics.[12] A comparison between the 5 fs and 40 fs data concluded essentially that no damage was observed within the longer pulse duration.[12] A systematic study of pulse duration on the radiation damage of SFX measurements of lysozyme microcrystals showed that pulses longer than 100 fs were damaging.[18] These measurements were however done under conditions of high absorbed dose on the GGy level.[18] Therefore, the lowest dose conditions that have been reported for successful high resolution SFX measurements were still at the ∼MGy level.[12] However, measurements with a second X-ray pulse which is time delayed by >1 ps has not been performed with SFX of micro-crystals. Whether radiation damage would develop on the picosecond time scale needed for a probe-pump-probe pulse sequence at the MGy level is yet to be determined. We therefore identify the ∼20 kGy dose as a dose that is likely to allow a second diffraction pattern to be collected, but experimental tests up to ∼MGy (but below the ∼10 MGy ablation threshold[17]) should be performed.

An additional consideration is that the beam overlap will be particularly critical in the case of SFX, which typically uses protein crystals with dimensions of 1–2 μm, which are comparable with the focus size. In this case, the I/σI value for a ratiometric measurement of Bragg reflection intensities is expected to degrade from a small jitter or a drift of the overlap. Such submicron precision challenges the mechanical stability of the SDL thus requiring stabilization through optical interferometric measurements (Table II).

VIII. SUMMARY AND DISCUSSION

A ratiometric measurement of the photo-induced structure factor amplitude differences ΔF done with a probe-pump-probe geometry as outlined in this article will be noise limited by photon counting statistics, provided that the replica beams stimulate the same mosaic blocks, and also provided that the split and delay lines perform stably on a shot-to-shot basis. It is concluded that XFEL experiments can be conducted under conditions of low absorbed dose that corresponds to those that are used at synchrotron stations.[5–11] The detection of femtosecond population transfer additionally depends on accurate and optimal coherent optical control. Optical parameters for femtosecond photolysis of PYP crystals were previously investigated[20] and implemented.[22]

The experiment will require a split-and-delay unit for femtosecond hard X-rays with a number of special characteristics, summarized in Table II and discussed in Sec. VI above. Currently, LCLS, SACLA, SwissFEL, and the European XFEL have hard X-ray split-and-delay units proposed or under design/commissioning. At LCLS, a focussing and dual mirror geometry has been established for soft X-ray experiments at the AMO beamline,[23] which is however not suitable for hard X-rays and delays longer than 200 fs. A hard X-ray split-and-delay unit based on thin crystals and high-order reflections has been developed and is under commissioning at LCLS.[47] The throughput of the device is about 2% in SASE mode and the outgoing beams are nearly collinear (54 μrad at 8.4 keV reported), which is not enough for the experiment proposed here. At SACLA, a Si(220) based split-and-delay unit is under construction with specifications very similar to the ones presented above for the MID instrument.[52] However, the SACLA design currently does not feature a suitable angular beam offset. A mirror-based SDL for the HED instrument at XFEL.EU is also in progress.[56] It is designed for photon energies of 5–20 keV and uses Mo/B_4C and Ni/B_4C multilayers as X-ray splitter, mirrors, and mixers, but also provides a co-linear geometry only. The MID station at XFEL.EU is therefore unique in its capability of accommodating the proposed probe-pump-probe scheme, additionally featuring high throughput allowing both single crystal and SFX studies. In terms of throughput, the requirement for a probe-pump-probe protein crystallography experiment using single crystals is approximately 10^{10} X-ray photons in each pulse replica[55] (Table II, second column). If the transmission of a crystal based beam splitter is too low, the diffraction intensities would be too weak to allow stroboscopic measurements with a limited number of pump-probe cycles for each frame. The self-seeding scheme that will be implemented at the European XFEL will lead to a much larger throughput of the SDL than in SASE mode and transmissions of 10% or higher can be expected.

The following considers a simple model to estimate the accuracy by which the photo-induced structure factor differences may be determined. While it was previously shown for applying the rotation method at XPP/LCLS, the crystallographic R_{meas} and signal-to-noise ratio $I/\sigma I$ may be estimated on the basis of source noise intensity measurements,[22] an internally referenced measurement proposed here would theoretically be limited by the dynamic range of the detector. Therefore, a theoretical crystallographic R factor, in the absence of source noise and other noise contributions, would correspond to the R_{meas} in the case of a single integrated Bragg reflection observation,[57] which would be collected in this scheme in a single frame. In this case, the $I/\sigma I$ value would correspond to the dynamic range and would estimate the R_{meas} value according to the following relationship:[57]

$$R_{meas} = \left(\frac{2}{\pi}\right)^{1/2} \frac{\langle \sigma_I \rangle}{\langle I_0 \rangle} \cong \frac{0.7979}{\langle I_0 \rangle / \langle \sigma_I \rangle} \tag{13}$$

This model predicts an R value of 0.02% for the MAR 165 detector, and would be similar for the AGIPD detector, provided that the full well capacity is used entirely. As discussed, instabilities of the pulse intensity ratio due to pointing, mode, and energy fluctuation of the split and delay unit would rapidly dominate the effective $I/\sigma I$ overshadowing the detector's dynamic range. Therefore, the use of dynamic range should be taken as the detector limited value only. Assuming, for example, an $I/\sigma I$ of 20 describing the intensity fluctuation assuming a Gaussian distribution, predicting an R value of 4% (see Eq. (13)).

The requirements for single crystal data collection under conditions of low absorbed dose, room temperature, and X-ray energy of 9 keV are satisfied by the design specifications of the SDL (Table II), which allow multiple diffraction events as the attenuated conditions are non-destructive under sufficient attenuation. The main questions to be addressed in considering whether a SFX application may be possible, concerns the absorbed dose and dose rate of the first pulse as well as the stability of the spatial overlap of the two micron-sized focused beam spots. We include SFX as a possible application because this may be favoured if high repetition rate measurements (available at the European XFEL) of weak signals give better statistics than low repetition rate measurements (for example, at LCLS, SwissFEL, and SACLA) of strong signals in the single crystal case.

Finally, it is noteworthy that a different type of "probe-pump-probe" experimental configuration was proposed for the ESC station at SwissFEL, but specifically for X-ray absorption spectroscopy.[58]

In conclusion, this manuscript has considered the experimental requirements for femtosecond time resolved X-ray protein crystallography, with an emphasis on internally referencing the SASE noise contributions of the XFEL in the experimental signal-to-noise of ΔF measurements. It is shown that there will be distinct advantage of this scheme not only just because of the expected high signal-to-noise but also because of the high experimental data correlation between unpumped and pumped dual-pattern frames.

ACKNOWLEDGMENTS

Portions of this research were carried out at the Linac Coherent Light Source (LCLS) at the SLAC National Accelerator Laboratory. LCLS is an Office of Science User Facility operated for the U.S. Department of Energy Office of Science by Stanford University. The LCLS is acknowledged for beam time access under Experiment Nos. xpp23410 and xpp44112. J.J.v.T. acknowledges support from EPSRC (via Award Nos. EP/I003304/1 and EP/M000192/1). A.M. acknowledges collaboration with Professor S. Eisebitt's group at TU-Berlin and the MID split-and-delay line funding obtained through a BMBF Verbundforschung grant (BMBF FSP 302 and 05K13KT4, "Split-X-MID"). We acknowledge stimulating discussions with Keith Moffat, Henry Chapman, and John Spence.

[1]G. E. Borgstahl, D. R. Williams, and E. D. Getzoff, "1.4 A structure of photoactive yellow protein, a cytosolic photoreceptor: Unusual fold, active site, and chromophore," Biochemistry **34**(19), 6278–6287 (1995).
[2]B. Perman, V. Srajer, Z. Ren, T. Teng, C. Pradervand, T. Ursby, D. Bourgeois, F. Schotte, M. Wulff, R. Kort, K. Hellingwerf, and K. Moffat, "Energy transduction on the nanosecond time scale: Early structural events in a xanthopsin photocycle," Science **279**(5358), 1946–1950 (1998).
[3]R. Neutze, R. Wouts, D. van der Spoel, E. Weckert, and J. Hajdu, "Potential for biomolecular imaging with femtosecond x-ray pulses," Nature **406**(6797), 752–757 (2000).
[4]F. Schotte, M. Lim, T. A. Jackson, A. V. Smirnov, J. Soman, J. S. Olson, G. N. Phillips, Jr., M. Wulff, and P. A. Anfinrud, "Watching a protein as it functions with 150-ps time-resolved x-ray crystallography," Science **300**(5627), 1944–1947 (2003).
[5]K. Moffat, "Time-resolved macromolecular crystallography," Annu. Rev. Biophys. Biophys. Chem. **18**, 309–332 (1989).
[6]Z. Ren and K. Moffat, "Laue crystallography for studying rapid reactions," J. Synchrotron Radiat. **1**(Pt 1), 78–82 (1994).
[7]K. Moffat, "Time-resolved crystallography," Acta Crystallogr., Sect. A **54**(1), 833–841 (1998).
[8]K. Moffat, "Time-resolved biochemical crystallography: A mechanistic perspective," Chem. Rev. **101**(6), 1569–1581 (2001).
[9]Z. Ren, B. Perman, V. Srajer, T. Y. Teng, C. Pradervand, D. Bourgeois, F. Schotte, T. Ursby, R. Kort, M. Wulff, and K. Moffat, "A molecular movie at 1.8 A resolution displays the photocycle of photoactive yellow protein, a eubacterial blue-light receptor, from nanoseconds to seconds," Biochemistry **40**(46), 13788–13801 (2001).
[10]B. Perman, S. Anderson, M. Schmidt, and K. Moffat, "New techniques in fast time-resolved structure determination," Cell Mol. Biol. (Noisy-le-grand) **46**(5), 895–913 (2000).
[11]R. Neutze and K. Moffat, "Time-resolved structural studies at synchrotrons and x-ray free electron lasers: Opportunities and challenges," Curr. Opin. Struct. Biol. **22**(5), 651–659 (2012).
[12]S. Boutet, L. Lomb, G. J. Williams, T. R. Barends, A. Aquila, R. B. Doak, U. Weierstall, D. P. DePonte, J. Steinbrener, R. L. Shoeman, M. Messerschmidt, A. Barty, T. A. White, S. Kassemeyer, R. A. Kirian, M. M. Seibert, P. A. Montanez, C. Kenney, R. Herbst, P. Hart, J. Pines, G. Haller, S. M. Gruner, H. T. Philipp, M. W. Tate, M. Hromalik, L. J. Koerner, N. van Bakel, J. Morse, W. Ghonsalves, D. Arnlund, M. J. Bogan, C. Caleman, R. Fromme, C. Y. Hampton, M. S. Hunter, L. C. Johansson, G. Katona, C. Kupitz, M. Liang, A. V. Martin, K. Nass, L. Redecke, F. Stellato, N. Timneanu, D. Wang, N. A. Zatsepin, D. Schafer, J. Defever, R. Neutze, P. Fromme, J. C. Spence, H. N. Chapman, and I. Schlichting, "High-resolution protein structure determination by serial femtosecond crystallography," Science **337**(6092), 362–364 (2012).
[13]R. A. Kirian, X. Wang, U. Weierstall, K. E. Schmidt, J. C. Spence, M. Hunter, P. Fromme, T. White, H. N. Chapman, and J. Holton, "Femtosecond protein nanocrystallography-data analysis methods," Opt. Express **18**(6), 5713–5723 (2010).
[14]H. N. Chapman, P. Fromme, A. Barty, T. A. White, R. A. Kirian, A. Aquila, M. S. Hunter, J. Schulz, D. P. DePonte, U. Weierstall, R. B. Doak, F. Maia, A. V. Martin, I. Schlichting, L. Lomb, N. Coppola, R. L. Shoeman, S. W. Epp, R. Hartmann, D. Rolles, A. Rudenko, L. Foucar, N. Kimmel, G. Weidenspointner, P. Holl, M. N. Liang, M. Barthelmess, C. Caleman, S. Boutet, M. J. Bogan, J. Krzywinski, C. Bostedt, S. Bajt, L. Gumprecht, B. Rudek, B. Erk, C. Schmidt, A. Homke, C. Reich, D. Pietschner, L. Struder, G. Hauser, H. Gorke, J. Ullrich, S. Herrmann, G. Schaller, F. Schopper, H. Soltau, K. U. Kuhnel, M. Messerschmidt, J. D. Bozek, S. P. Hau-Riege, M. Frank, C. Y. Hampton, R. G. Sierra, D. Starodub, G. J. Williams, J. Hajdu, N. Timneanu, M. M. Seibert, J. Andreasson, A. Rocker, O. Jonsson, M. Svenda, S. Stern, K. Nass, R. Andritschke, C. D. Schroter, F. Krasniqi, M. Bott, K. E. Schmidt, X. Y. Wang, I. Grotjohann, J. M. Holton, T. R. M. Barends, R. Neutze, S. Marchesini, R. Fromme, S. Schorb, D. Rupp, M. Adolph, T. Gorkhover, I. Andersson, H. Hirsemann, G. Potdevin, H. Graafsma, B. Nilsson, and J. C. H. Spence, "Femtosecond x-ray protein nanocrystallography," Nature **470**(7332), 73–U81 (2011).
[15]C. Kupitz, S. Basu, I. Grotjohann, R. Fromme, N. A. Zatsepin, K. N. Rendek, M. S. Hunter, R. L. Shoeman, T. A. White, D. Wang, D. James, J. H. Yang, D. E. Cobb, B. Reeder, R. G. Sierra, H. Liu, A. Barty, A. L. Aquila, D. Deponte, R. A. Kirian, S. Bari, J. J. Bergkamp, K. R. Beyerlein, M. J. Bogan, C. Caleman, T. C. Chao, C. E. Conrad, K. M. Davis, H. Fleckenstein, L. Galli, S. P. Hau-Riege, S. Kassemeyer, H. Laksmono, M. Liang, L. Lomb, S. Marchesini, A. V. Martin, M. Messerschmidt, D. Milathianaki, K. Nass, A. Ros, S. Roy-Chowdhury, K. Schmidt, M. Seibert, J. Steinbrener, F. Stellato, L. Yan, C. Yoon, T. A. Moore, A. L. Moore, Y. Pushkar, G. J. Williams, S. Boutet, R. B. Doak, U. Weierstall, M. Frank, H. N. Chapman, J. C. Spence, and P. Fromme, "Serial time-resolved crystallography of photosystem II using a femtosecond x-ray laser," Nature **513**, 261 (2014).
[16]A. Aquila, M. S. Hunter, R. B. Doak, R. A. Kirian, P. Fromme, T. A. White, J. Andreasson, D. Arnlund, S. Bajt, T. R. Barends, M. Barthelmess, M. J. Bogan, C. Bostedt, H. Bottin, J. D. Bozek, C. Caleman, N. Coppola, J. Davidsson, D. P. DePonte, V. Elser, S. W. Epp, B. Erk, H. Fleckenstein, L. Foucar, M. Frank, R. Fromme, H. Graafsma, I. Grotjohann, L. Gumprecht, J. Hajdu, C. Y. Hampton, A. Hartmann, R. Hartmann, S. Hau-Riege, G. Hauser, H. Hirsemann, P. Holl, J. M. Holton, A. Homke, L. Johansson, N. Kimmel, S. Kassemeyer, F. Krasniqi, K. U. Kuhnel, M. Liang, L. Lomb, E. Malmerberg, S. Marchesini, A. V. Martin, F. R. Maia, M. Messerschmidt, K. Nass, C. Reich, R. Neutze, D. Rolles, B. Rudek, A. Rudenko, I. Schlichting, C. Schmidt, K. E. Schmidt, J. Schulz, M. M. Seibert, R. L. Shoeman, R. Sierra, H. Soltau, D. Starodub, F. Stellato, S. Stern, L. Struder, N. Timneanu, J. Ullrich, X. Wang, G. J. Williams, G. Weidenspointner, U. Weierstall, C. Wunderer, A. Barty, J. C. Spence, and H. N. Chapman, "Time-resolved protein nanocrystallography using an x-ray free-electron laser," Opt. Express **20**(3), 2706–2716 (2012).
[17]H. N. Chapman, C. Caleman, and N. Timneanu, "Diffraction before destruction," Philos. Trans. R. Soc. London, Ser. B **369**(1647), 20130313 (2014).
[18]L. Lomb, T. R. M. Barends, S. Kassemeyer, A. Aquila, S. W. Epp, B. Erk, L. Foucar, R. Hartmann, B. Rudek, D. Rolles, A. Rudenko, R. L. Shoeman, J. Andreasson, S. Bajt, M. Barthelmess, A. Barty, M. J. Bogan, C. Bostedt, J. D. Bozek, C. Caleman, R. Coffee, N. Coppola, D. P. DePonte, R. B. Doak, T. Ekeberg, H. Fleckenstein, P. Fromme, M. Gebhardt, H. Graafsma, L. Gumprecht, C. Y. Hampton, A. Hartmann, G. n. Hauser, H. Hirsemann, P. Holl, J. M. Holton, M. S. Hunter, W. Kabsch, N. Kimmel, R. A. Kirian, M. Liang, F. R. N. C. Maia, A. Meinhart, S. Marchesini, A. V. Martin, K. Nass, C. Reich, J. Schulz, M. M. Seibert, R. Sierra, H. Soltau, J. C. H. Spence, J. Steinbrener, F. Stellato, S. Stern, N. Timneanu, X. Wang, G. Weidenspointner, U. Weierstall, T. A. White, C. Wunderer, H. N. Chapman, J. Ullrich, L. Strueder, and I.

Schlichting, "Radiation damage in protein serial femtosecond crystallography using an x-ray free-electron laser," Phys. Rev. B **84**(21), 214111 (2011).
[19]J. Kern, R. Alonso-Mori, R. Tran, J. Hattne, R. J. Gildea, N. Echols, C. Glockner, J. Hellmich, H. Laksmono, R. G. Sierra, B. Lassalle-Kaiser, S. Koroidov, A. Lampe, G. Han, S. Gul, D. Difiore, D. Milathianaki, A. R. Fry, A. Miahnahri, D. W. Schafer, M. Messerschmidt, M. M. Seibert, J. E. Koglin, D. Sokaras, T. C. Weng, J. Sellberg, M. J. Latimer, R. W. Grosse-Kunstleve, P. H. Zwart, W. E. White, P. Glatzel, P. D. Adams, M. J. Bogan, G. J. Williams, S. Boutet, J. Messinger, A. Zouni, N. K. Sauter, V. K. Yachandra, U. Bergmann, and J. Yano, "Simultaneous femtosecond x-ray spectroscopy and diffraction of photosystem II at room temperature," Science **340**(6131), 491–495 (2013).
[20]C. N. Lincoln, A. E. Fitzpatrick, and J. J. van Thor, "Photoisomerisation quantum yield and non-linear cross-sections with femtosecond excitation of the photoactive yellow protein," Phys. Chem. Chem. Phys. **14**(45), 15752–15764 (2012).
[21]T. R. Barends, L. Foucar, S. Botha, R. B. Doak, R. L. Shoeman, K. Nass, J. E. Koglin, G. J. Williams, S. Boutet, M. Messerschmidt, and I. Schlichting, "De novo protein crystal structure determination from x-ray free-electron laser data," Nature **505**(7482), 244–247 (2013).
[22]J. J. van Thor, M. M. Warren, C. N. Lincoln, M. Chollet, H. T. Lemke, D. M. Fritz, M. Schmidt, J. Tenboer, Z. Ren, V. Srajer, K. Moffat, and T. Graber, "Signal to noise considerations for single crystal femtosecond time resolved crystallography of the photoactive yellow protein," Faraday Discuss. **171**, 439 (2014).
[23]J. C. Castagna, B. Murphy, J. Bozek, and N. Berrah, "X-ray split and delay system for soft x-ray at LCLS," J. Phys.: Conf. Ser. **425**, 152021 (2013).
[24]S. Roling, S. Braun, P. Gawlitza, L. Samoylova, B. Siemer, H. Sinn, F. Siewert, F. Wahlert, M. Wostmann, and H. Zacharias, "A split- and delay-unit for the European XFEL," Proc. SPIE **8778**, 87781G (2013).
[25]F. Sorgenfrei, W. F. Schlotter, T. Beeck, M. Nagasono, S. Gieschen, H. Meyer, A. Fohlisch, M. Beye, and W. Wurth, "The extreme ultraviolet split and femtosecond delay unit at the plane grating monochromator beamline PG2 at FLASH," Rev. Sci. Instrum. **81**(4), 043107 (2010).
[26]B. Fournier and P. Coppens, "On the assessment of time-resolved diffraction results," Acta Crystallogr., Sect. A **70**(Pt 3), 291–299 (2014).
[27]M. Rossmann, "Processing oscillation diffraction data for very large unit cells with an automatic convolution technique and profile fitting," J. Appl. Crystallogr. **12**(2), 225–238 (1979).
[28]M. G. Rossmann, A. G. W. Leslie, S. S. Abdel-Meguid, and T. Tsukihara, "Processing and post-refinement of oscillation camera data," J. Appl. Crystallogr. **12**(6), 570–581 (1979).
[29]A. G. Leslie, "Integration of macromolecular diffraction data," Acta Crystallogr., Sect. D: Biol. Crystallography **55**(Pt 10), 1696–1702 (1999).
[30]J. X. Ho, J. R. Ruble, T. R. McInnis, D. C. Carter, H. Huang, and W. M. Gibson, "Convergent-beam method in macromolecular crystallography," Acta Crystallogr., Sect. D: Biol Crystallogr. **58**(Pt 12), 2087–2095 (2002).
[31]J. X. Ho, E. H. Snell, R. C. Sisk, J. R. Ruble, D. C. Carter, S. M. Owens, and W. M. Gibson, "Stationary crystal diffraction with a monochromatic convergent x-ray source and application for macromolecular crystal data collection," Acta Crystallogr., Sect. D: Biol. Crystallogr. **54**(Pt 2), 200–214 (1998).
[32]T. A. White, "Post-refinement method for snapshot serial crystallography," Philos. Trans. R. Soc. London, Ser. B **369**(1647), 20130330 (2014).
[33]J. C. Spence, N. A. Zatsepin, and C. Li, "Coherent convergent-beam time-resolved x-ray diffraction," Philos. Trans. R. Soc. London, Ser. B **369**(1647), 20130325 (2014).
[34]C. A. MacDonald, S. M. Owens, and W. M. Gibson, "Polycapillary x-ray optics for microdiffraction," J. Appl. Crystallogr. **32**(2), 160–167 (1999).
[35]W. Kabsch, "XDS," Acta Crystallogr., Sect. D: Biol Crystallogr. **66**(Pt 2), 125–132 (2010).
[36]M. D. Winn, C. C. Ballard, K. D. Cowtan, E. J. Dodson, P. Emsley, P. R. Evans, R. M. Keegan, E. B. Krissinel, A. G. Leslie, A. McCoy, S. J. McNicholas, G. N. Murshudov, N. S. Pannu, E. A. Potterton, H. R. Powell, R. J. Read, A. Vagin, and K. S. Wilson, "Overview of the CCP4 suite and current developments," Acta Crystallogr., Sect. D: Biol. Crystallogr. **67**(Pt 4), 235–242 (2011).
[37]T. J. Greenhough and J. R. Helliwell, "Oscillation camera data processing: Reflecting range and prediction of partiality. 1. Conventional x-ray sources," J. Appl. Crystallogr. **15**, 338–351 (1982).
[38]F. K. Winkler, C. E. Schutt, and S. C. Harrison, "The oscillation method for crystals with very large unit cells," Act Crystallogr., A **35**, 901–911 (1979).
[39]T. A. White, A. Barty, F. Stellato, J. M. Holton, R. A. Kirian, N. A. Zatsepin, and H. N. Chapman, "Crystallographic data processing for free-electron laser sources," Acta Crystallogr., Sect. D: Biol. Crystallogr. **69**(Pt 7), 1231–1240 (2013).
[40]K. Diederichs, "Simulation of x-ray frames from macromolecular crystals using a ray-tracing approach," Acta Crystallogr., Sect. D: Biol. Crystallogr. **65**(Pt 6), 535–542 (2009).
[41]R. C. Agarwal, "A new least-squares refinement technique based on the fast Fourier transform algorithm," Act Crystallogr., A **34**, 791–809 (1978).
[42]S. Tripathi, V. Srajer, N. Purwar, R. Henning, and M. Schmidt, "pH dependence of the photoactive yellow protein photocycle investigated by time-resolved crystallography," Biophys. J. **102**(2), 325–332 (2012).
[43]A. Madsen, J. Hallmann, T. Roth, and G. Ansaldi, "Technical design report: Scientific instrument MID," DESY-2013-00872, 2013.
[44]D. Greiffenberg, J. Becker, L. Bianco, R. Dinapoli, P. Goettlicher, H. Graafsma, H. Hirsemann, S. Jack, R. Klanner, A. Klyuev, H. Kruger, S. Lange, A. Marras, A. Mozzanica, S. Rah, B. Schmitt, J. Schwandt, I. Sheviakov, X. Shi, U. Trunk, J. Zhang, M. Zimmer, D. Mezza, A. Allahgholi, and Q. Xia, "Towards AGIPD1.0: Optimization of the dynamic range and investigation of a pixel input protection," J. Instrum. **9**(06), P06001 (2014).
[45]H. Graafsma, "Requirements for and development of 2 dimensional x-ray detectors for the European x-ray free electron laser in Hamburg," JINST **4**, P12011 (2009).
[46]L. Bianco, J. Becker, R. D. Dinapoli, E. Fretwurst, P. Goettlicher, H. Graafsma, D. Greiffenberg, M. Gronewald, B. Henrich, H. Hirsemann, S. Jack, R. Klanner, A. Klyuev, H. Krueger, A. Marras, A. Mozzanica, S. Rah, B. Schmitt, X. Shi, U. Trunk, J. Schwandt, and J. Zhang, "The AGIPD System for the European XFEL," Proc. SPIE **8778**, 87780V (2013).

[47]W. Roseker, H. Franz, H. Schulte-Schrepping, A. Ehnes, O. Leupold, F. Zontone, S. Lee, A. Robert, and G. Grubel, "Development of a hard x-ray delay line for x-ray photon correlation spectroscopy and jitter-free pump-probe experiments at x-ray free-electron laser sources," J. Synchrotron Radiat. **18**(Pt 3), 481–491 (2011).
[48]W. Roseker, H. Franz, H. Schulte-Schrepping, A. Ehnes, O. Leupold, F. Zontone, A. Robert, and G. Grubel, "Performance of a picosecond x-ray delay line unit at 8.39 keV," Opt. Lett. **34**(12), 1768–1770 (2009).
[49]W. Roseker, S. Lee, M. Walther, H. Schulte-Schrepping, H. Franz, A. Gray, M. Sikorski, P. H. Fuoss, G. B. Stephenson, A. Robert, and G. Grubel, "Hard x-ray delay line for x-ray photon correlation spectroscopy and jitter-free pump-probe experiments at LCLS," Proc. SPIE **8504**, 85040I (2012).
[50]J. Amann, W. Berg, V. Blank, F.-J. Decker, Y. Ding, P. Emma, Y. Feng, J. Frisch, D. Fritz, J. Hastings, Z. Huang, I. J. Krzywinsk, R. Lindberg, H. Loos, A. Lutman, H. D. Nuhn, D. Ratner, J. Rzepiela, D. Shu, Y. Shvyd'ko, S. Spampinati, S. Stoupin, S. Terentyev, E. Trakhtenberg, D. Walz, J. Welch, J. Wu, A. Zholents, and D. Zhu, "Demonstration of self-seeding in a hard-x-ray free-electron laser," Nat. Photonics **6**(10), 693–698 (2012).
[51]G. Geloni, V. Kocharyan, and E. Saldin, "A novel self-seeding scheme for hard x-ray FELs," J. Mod. Opt. **58**(16), 1391–1403 (2011).
[52]T. Osaka, M. Yabashi, Y. Sano, K. Tono, Y. Inubushi, T. Sato, S. Matsuyama, T. Ishikawa, and K. Yamauchi, "A Bragg beam splitter for hard x-ray free-electron lasers," Opt. Express **21**(3), 2823–2831 (2013).
[53]R. Henderson, "Cryo-protection of protein crystals against radiation damage in electron and x-ray diffraction," Proc. R. Soc. London, Ser. B **241**(1300), 6–8 (1990).
[54]R. Henderson, "The potential and limitations of neutrons, electrons and x-rays for atomic resolution microscopy of unstained biological molecules," Q. Rev. Biophys. **28**(2), 171–193 (1995).
[55]T. Graber, S. Anderson, H. Brewer, Y. S. Chen, H. S. Cho, N. Dashdorj, R. W. Henning, I. Kosheleva, G. Macha, M. Meron, R. Pahl, Z. Ren, S. Ruan, F. Schotte, V. Srajer, P. J. Viccaro, F. Westferro, P. Anfinrud, and K. Moffat, "BioCARS: A synchrotron resource for time-resolved x-ray science," J. Synchrotron Radiat. **18**(Pt 4), 658–670 (2011).
[56]M. Nakatsutsumi and T. Tschentscher, "Conceptual design report scientific instrument high energy density physics (HED)," XFEL.EU TR-2013-003, 2013.
[57]K. Diederichs and P. A. Karplus, "Improved R-factors for diffraction data analysis in macromolecular crystallography," Nat. Struct. Biol. **4**(4), 269–275 (1997).
[58]B. D. Patterson and R. Abela, "Novel opportunities for time-resolved absorption spectroscopy at the x-ray free electron laser," Phys. Chem. Chem. Phys. **12**(21), 5647–5652 (2010).